Dalton Transactions

Accepted Manuscript

ROYAL SOCIETY OF CHEMISTRY

www.rsc.org/dalton

Dalton Transactions

RSCPublishing

ARTICLE

Structure and photoluminescence properties of a rare-earth free red-emitting Mn^{2+}-activated $KMgBO_3$

Cite this: DOI: 10.1039/x0xx00000x

L. Wu[a], B. Wang[a, b], Y. Zhang[b*], L. Li[c], H. R. Wang[b], H. Yi[a], Y. F. Kong[a] and J. J. Xu[a]

Received 00th January 2012,
Accepted 00th January 2012

DOI: 10.1039/x0xx00000x

www.rsc.org/

In this combined X-ray diffraction and photoluminescence study, the coordination environment of Mn^{2+} and the photoluminescence of single Mn^{2+} doped $KMgBO_3$ phosphors were studied. Mn^{2+} occupies Mg^{2+} site, which were coordinated by six O^{2-}. The strong absorption of $KMgBO_3$:Mn^{2+} was ascribed to the strong relaxation of spin and parity forbidden of Mn^{2+}. The emission bands were centered at 636 nm, regardless of the excitation wavelength and Mn^{2+} doping concentration. Mn^{2+} activated $KMgBO_3$ could be efficiently excited with the excitation of Mn^{2+} d-d transitions in the wavelength range of 300-475 nm. The red-shift of Mn^{2+} emission was because of strong crystal field environment of Mn^{2+} afforded by $KMgBO_3$. The potential applications of the phosphors had been pointed out based on the absorption spectra, excitation and emission spectra, thermal quenching properties, and decay properties.

1. Introduction

Mn^{2+}, a transition metal ion, has been playing an important role in modern lighting and display fields.[1-4] Divalent manganese (Mn^{2+}) ion has a d^5 configuration. From the Tanabe-Sugano diagrams, it can be derived that emission corresponds to the $^4T_1$ to $^6A_1$ transition. The position of the lowest excited state strongly depends on the crystal field strength, which allows shifting the Mn^{2+} emission from green to red, depending on the crystal field strength of the substituted sites.[5] The emission of Mn^{2+} originates from parity-forbidden d-d transitions. As a consequence, the absorption is very weak. Since the excited levels of Mn^{2+} match some energy levels of the lanthanides (such as Eu^{2+} and Ce^{3+}), the efficient energy transfer from the codoping lanthanide ions to Mn^{2+} takes place, resulting in the intensities of emission band of Mn^{2+} ions increasing.[6,7] However, rare earth elements used in these luminescent centers of the phosphors are typically expensive. In order to develop the inexpensive materials with good luminescence performance, great efforts to investigate the Mn^{2+} single doped compounds have been carried out and some Mn^{2+} doped phosphors with very good luminescence properties have been synthesized successfully, such as β-$Zn_3B_2O_6$:Mn^{2+} [4], $LiZnPO_4$:Mn^{2+},[8] MZnOS:Mn^{2+}(M=Ca, Ba),[9] Li_2ZnGeO_4:Mn^{2+},[10] and so on. These researches indicate that the hosts which can afford strong crystal field to Mn^{2+} ion are crucial for the Mn^{2+} single doped phosphors with good properties. However, up to now, the hosts used to synthesize the Mn^{2+} doped phosphors are almost Zn-based compounds. As for other ion-based compounds, such as Mg-based compounds, there is seldom reported Mn^{2+} single doped phosphor with good performance.[11]

Borates constitute attractive classes of host lattices for emitting *d* or *f* electrons due to their excellent thermal stability, chemical stability, and wide band gaps. Phosphors based on borates show excellent luminescence performance because of their abundant structures which can afford different crystal fields for the *d* or *f* metal cations to tune the luminescence properties.[12,13] For example, $KSr_4(BO_3)_3$ crystallizes in space group *Ama*2, in which there are 4 crystallographically independent cation sites with different coordination environments.[14] It supplies a great potential to design new phosphors by doping different ions, such as Eu^{3+}, Dy^{3+}, and Tm^{3+},[15,16] and generate phosphor with tunable light from blue, white to red color; $NaSrBO_3$ crystallizes in the monoclinic space group $P2_1/c$, in which one Sr^{2+} ion is surrounded by nine O^{2-} ions. By doping Ce^{3+} in Sr^{2+} sites, a blue-emitting phosphor which is used to fabricate LED successfully is synthesized.[17]

As a member of the borates, $KMgBO_3$ was first reported to be crystallized in a cubic system with space group $P2_13$ under ambient pressure by our group in 2010.[18] $KMgBO_3$ offers the possible substitution positions for Mn^{2+} cation considering the ionic radius, including K^+ site and Mg^{2+} site. It is interesting that K^+ and Mg^{2+} are all coordinated with six O^{2-} to form the distorted octahedron, which can afford strong crystal field for doped Mn^{2+}. So $KMgBO_3$ will be a good host to be doped by Mn^{2+}. In this study, the photoluminescence performance of $KMgBO_3$ doped by Mn^{2+} is studied based on the structure and surroundings of Mn^{2+}. An unusual strong absorption is

observed and a red-emitting phosphor is synthesized, which is a potential red phosphor in LED lighting.

2. Experimental

2.1 Synthesis

The $KMgBO_3:xMn^{2+}$ (x=0.07, 0.08, 0.09, 0.10, 0.11, 0.12, 0.13) powders were prepared by high temperature solid-state reaction method. The starting materials K_2CO_3(99.9%), MgO(99.9%), H_3BO_3(99.9%), $MnCO_3$(99.9%) were accurately weighted and ground in an agate mortar. The well-mixed materials were first pre-sintered at 550°C for 24h. Then the obtained samples were thoroughly mixed, ground and transferred to an alumina boat, and heated at 800°C under a reducing atmosphere ($5H_2$/95Ar) for 8h.

2.2 Characterizations

The XRD data for phase identification and structural refinements were collected at ambient temperature using a PANalytical powder X-ray diffractometer X'Pert Pro with Cu-Kα radiation (40 kV, 40 mA). The data were collected over a 2θ range from 10° to 135° at intervals of 0.017° with a counting time of 1s per step. The diffuse reflection spectrum was recorded using a UV-Vis-NIR spectrophotometer (U4100, HITACHI, Japan) using the white $BaSO_4$ powder as a references standard. The photoluminescence (PL) and photoluminescence excitation (PLE) spectra were measured by a spectrofluorometer (Edinburgh Instruments, FLS920) equipped with a Xe light source and double excitation monochromators. A μF900 laser (100 W) was used as a light source for the emission lifetimes measurement. The temperature-dependent luminescence properties were measured on an F-4600 spectrophotometer, which was equipped with a computer-controlled electric furnace. The internal quantum efficiency of optimized-composition phosphor $KMgBO_3:0.09Mn^{2+}$ was determined on an FLS920 spectrometer under excitation of 438 nm.

3. Results and Discussion

3.1 Structure of $KMgBO_3:Mn^{2+}$ phosphor

Fig. 1(a) shows the XRD patterns of $KMgBO_3:Mn^{2+}$ phosphors. All XRD patterns are found to agree well with that reported in the Inorganic Crystal Stucture Database (ICSD 174336), indicating that the doped Mn^{2+} ions do not generate any impurity or induce significant changes in the host structure.

$KMgBO_3$ crystallizes in a cubic system with space group $P2_13$ and the lattice parameters of a=6.8344(1) Å, V=319.23(1) Å^3, and Z=4. The crystal structure of $KMgBO_3$ offers two types of sites for the occupancy of Mn^{2+} ions: K^+ site (4a) in distorted [KO_6] polyhedra and Mg^{2+} site (4a) in distorted [MgO_6] polyhedra. The ionic radii of Mn^{2+} is 0.83 when CN=6. Compared with the radii of K^+ (1.38 Å when CN=6) and Mg^{2+} (r=0.72 Å when CN=6),[19] Mn^{2+} is preferred to occupy Mg^{2+} site. Other than the difference in valence, the radius of K^+ is much larger than that of Mn^{2+}, which will result in the crystal structure distortion of $KMgBO_3$ too much to be stable in crystallography if the K^+ site is occupied by Mn^{2+}. Therefore, Mn^{2+} will not prefer to occupy K^+ sites in this compound.

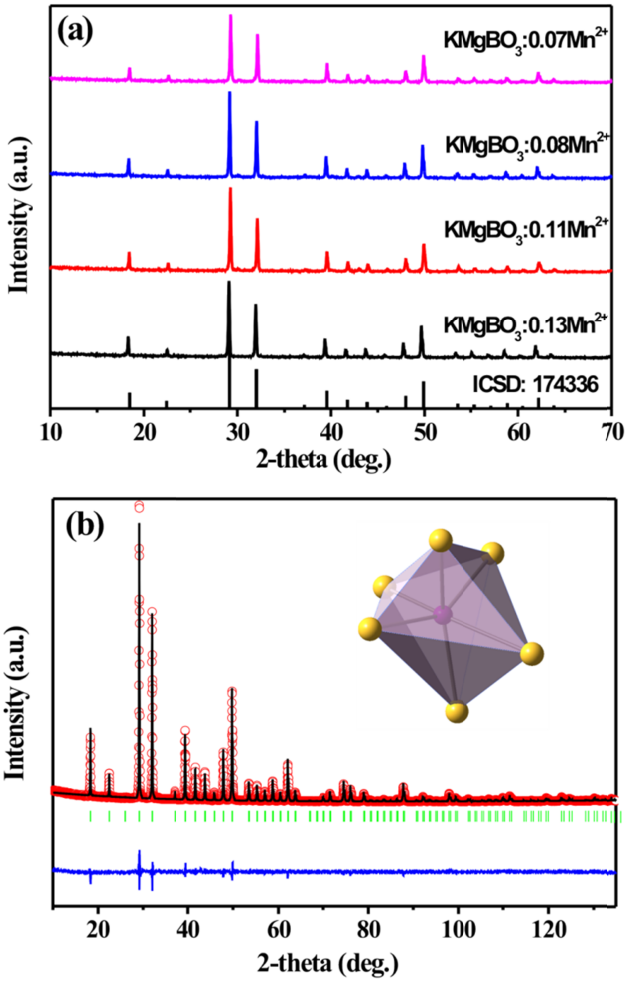

Fig. 1. (a) The XRD patterns of $KMgBO_3:Mn^{2+}$ phosphors with different Mn^{2+} doping contents. (b) Rietveld refinement result of $KMgBO_3:09Mn^{2+}$. Small circles (o) correspond to experiment values; and the continuous lines refers to the calculated pattern; vertical bars (|) indicate the position of Bragg Peaks; the bottom trace depicts the difference between the experimental and the calculated intensity values. The inset in (b) is the structure of [MgO_6] octahedron.

In order to prove the Mn^{2+} ions occupying Mg^{2+} site, structure refinement of the $KMgBO_3:0.09Mn^{2+}$ is performed using the structure of $KMgBO_3$ as the initial structure model by Rietveld method [22,23] within the Fullprof Program [24]. The final agreement factor converged to R_p=6.53%, R_{wp}=8.41%, and R_{exp}=4.41%. Fig.1(b) is the final Rietveld refinement plot of $KMgBO_3:0.09Mn^{2+}$, and the inset is the structure of [MgO_6] octahedra. The refinement results are listed in Table 1 and 2. The refined concentration of Mn^{2+} is 8.47mol % (Table S1), which is in good agreement with the original doping concentration of 9%. The lattice parameters (Table S1) of the doped sample become larger than those of the undoped compound, and the average bond distance of Mg(Mn)-O

(2.1269 Å, Table S2) is also longer than that of Mg-O (2.1225 Å) in $KMgBO_3$. These results are consistent with the case that $r_{Mn^{2+}}$ is larger than $r_{Mg^{2+}}$. The Rietveld refinement results confirm that Mn^{2+} ions occupy Mg^{2+} (4a) site, which means one Mn^{2+} ion is coordinated by 6 O^{2-} in $KMgBO_3$ with an octahedral crystal field environment.

3.2 Photoluminescence properties of $KMgBO_3:Mn^{2+}$

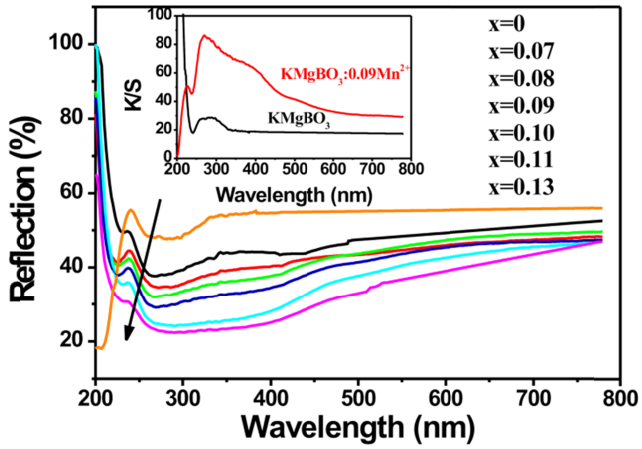

Fig. 2. Diffuse reflection spectra of $KMgBO_3:xMn^{2+}$ sample. Inset shows the absorption spectrum (K/S) of $KMgBO_3$ and $KMgBO_3$:0.09Mn^{2+} derived with the Kubelka-Munk function.

Fig. 2 shows the diffuse reflection spectra of the undoped and Mn^{2+}-doped $KMgBO_3$ samples. The absorption in the range below 240 nm is the ultraviolet absorption of host. In the region of 240-320 nm, there is an obvious decrease, which is ascribed to the charge transfer state (CTS) of O^{2-}–Mn^{2+} transition. The absorption in the region of 300-500 nm is mainly from d-d transition of Mn^{2+}.[9] The energy absorption is in the range from 240 nm to 500 nm and the reflection intensities are weaken with the Mn^{2+} concentration increasing, i.e., the absorptions of Mn^{2+} doped $KMgBO_3$ samples become stronger with the increase of the Mn^{2+} concentration, and several peaks in the range from 320 to 500 nm become obvious for the sample of doping concentration higher than 9 mol%. To better understand the absorptions of undoped and doped samples, the absorption spectra of $KMgBO_3:xMn^{2+}$ (x=0, 0.09) are obtained from the reflection spectra using the Kubelka-Munk function[23]

$$F(R) = (1-R)^2/2R = K/S \quad (1)$$

where R, K, and S refers to reflection, absorption, and scattering coefficient, respectively. In the derived absorption spectrum (K/S) of $KMgBO_3$ with Eq. (1) (inset of Fig. 2), two absorption bands can be observed in the wavelength range below 320 nm. The peak in the wavelength range below 240 nm belongs to the host absorption and the band gap should be larger than 6.2 eV (200 nm) (the edge is beyond the detection of our instrument), which indicates $KMgBO_3$ is a good candidate from the consideration of band gap. Because of the intense reflection, the undoped $KMgBO_3$ shows a white daylight color. For the Mn^{2+} doped samples, they show white to pink color varying with increasing Mn^{2+} concentration because of the strong absorption in the range of 320-550 nm, as the absorption spectra of $KMgBO_3$:0.09Mn^{2+} shown in the inset of Fig. 2. The peak in the range of 200-240 nm belongs to the host absorption, while the peak centered at 267 nm belongs to CTS. There are some broad peaks in the range of 340-550 nm, which originate from d-d transition of Mn^{2+}. Because the d-d transition of Mn^{2+} are spin and parity forbidden, the absorption band of Mn^{2+} in $KMgBO_3$ are expected to be weak, as observed in $ZnGeN_2$.[24] However, the intensity of the emission band of Mn^{2+} is strong. As indicated in the inset of Fig. 1(b), the coordinated octahedron of Mn^{2+} is distorted, and the crystal field of Mn^{2+} is strong. The strong crystal field will lead to the level splitting of Mn^{2+}, which will result in the relaxation of spin and parity forbidden. So the unexpectedly strong absorption of Mn^{2+} in $KMgBO_3$ can be attributed to that the spin and parity selection rules are shifted to a considerable extent, similar with that in CaZnOS.[9]

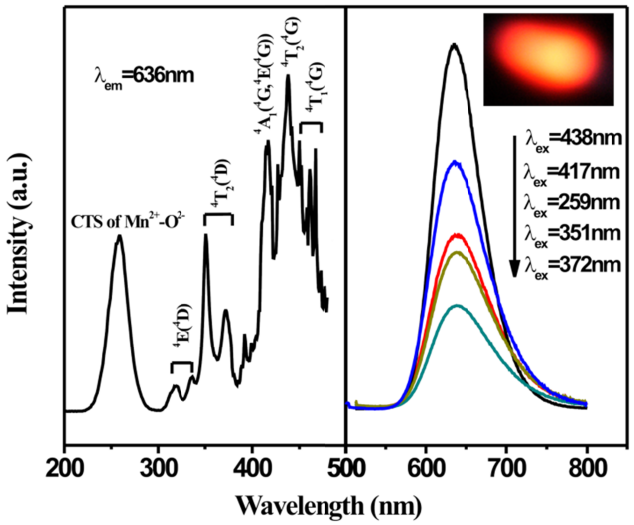

Fig. 3. Typical excitation spectra monitored at 636nm and emission spectra excited at different wavelength of $KMgBO_3$:0.09Mn^{2+} phosphor. Inset is the corresponding luminescence photograph for the sample excited at 351 nm in the dark with bright red color to the naked eye.

The PL and PLE spectra of $KMgBO_3:Mn^{2+}$ are shown in Fig. 3. Monitored at 636 nm, the PLE spectra consists of CTS band peaking at 259 nm and several linear peaks in the range from 300-475 nm, supported by the diffuse reflection spectrum (Fig. 2). The CTS band originates from the transformation of electron on $2p^6$ orbit of O^{2-} to $3d^5$ orbit of Mn^{2+}. The other excitation peaks in the range from 300 to 475 nm originate from the 3d-3d transition of Mn^{2+}. According to Orgel's diagram,[25] the two weak bands in the range of 300-340 nm are corresponding to $^6A_1 \rightarrow {}^4E(^4D)$, and the bands in the region from 340 to 380 nm originate from the splitting of $^6A_1 \rightarrow {}^4T_2(^4D)$. The sharp peak centered at 417 nm is corresponding to $^6A_1 \rightarrow [{}^4A_1(^4G), {}^4E(^4G)]$. The peak centered at 438 nm is corresponding to $^6A_1 \rightarrow {}^4T_2(^4G)$, and the other peaks in the range of 450-470

nm are corresponding to $^6A_1 \rightarrow {}^4T_1(^4G)$. These designations are coincident with those reported in Ref. 26.

Normally, the emission color is strongly dependent on the coordination environment of Mn^{2+} in the host lattice. Tetrahedrally coordinated Mn^{2+} usually gives a green emission, while octahedrally coordinated Mn^{2+} gives an orange to deep red emission. Mn^{2+} is distorted octahedral coordination in $KMgBO_3$. As a consequence, red emissions are observed in the Mn^{2+} activated $KMgBO_3$ phosphor, as PL spectra shown in Fig. 3. The red emission bands in the wavelength of 550-750 nm are centered at about 636 nm, regardless of the excitation wavelength. The observed band emission is ascribed to the $^4T_1(^4G) \rightarrow {}^6A_1(^6S)$ transition of Mn^{2+} incorporated in the $KMgBO_3$ host lattice. Both the peak position and the shape of the emission spectrum are independent of excitation wavelength, which indicate that there is only one emission center in the phosphor and confirm that the activator ions (Mn^{2+}) occupy only one type of equivalent positions in the $KMgBO_3$ host lattice. The full width of half maximum (FWHM) of emission band excited at 438 nm is 70 nm, which is close to the FWHM of CaZnOS:Eu^{2+} (60 nm), a red emitting phosphor successfully used in LED lighting.[27] Smet et al. indicate that the red color with 70 nm FWHM is very good to fabricate LED lighting with green and blue color with good color rendering and the luminous efficiency of the radiation.[3] Compared with β-$Zn_3(PO_4)_2$:Mn^{2+} (λ_{em}=616 nm) and $LaMg_{0.97}Mn_{0.03}B_5O_{10}$ (λ_{em}=616 nm), the maximum wavelength of $KMgBO_3$:Mn^{2+} is 636 nm, longer than those in β-$Zn_3(PO_4)_2$:Mn^{2+} and $LaMg_{0.97}Mn_{0.03}B_5O_{10}$ (the maximum wavelength of β-$Zn_3(PO_4)_2$:Mn^{2+} and $LaMg_{0.97}Mn_{0.03}B_5O_{10}$ are λ_{em}=616 nm and λ_{em}=620 nm, respectively). As described by Shi et al. and Wang et al.,[4,26] this can be ascribed to the effect of the strong crystal field.

Normally, the intensities of the excitation bands of Mn^{2+} are very weak because d-d transitions of Mn^{2+} are spin and parity forbidden, so are the intensities of the emission peaks in the Mn^{2+} single doped phosphors. In order to enhance the emission intensity of Mn^{2+}, normally a sensitizer will be co-doped to increase the excitation/absorption of Mn^{2+}, such as $RbMgF_3$:Eu^{2+},Mn^{2+},[28] $Ba_3MgSi_2O_8$:Eu^{2+},Mn^{2+},[29] and $CaAl_2Si_2O_8$:Eu^{2+},Mn^{2+}.[30] However, in this study, the intensities of the excitation bands of Mn^{2+} itself are very strong without any other codoped rare earth ions to transfer energy, especially the intensity of excitation band centered at 438 nm is even stronger than that of CTB in $KMgBO_3$:Mn^{2+}, so is the intensity of the emission band ($KMgBO_3$:Mn^{2+} excited at 351 nm UV lamp shows strong red color, as shown in the inset of Fig. 3). The strong intensities can be ascribed to a high absorption and a high quantum efficiency of Mn^{2+} in the host lattice, which is similar to that in the CaZnOS host.[9] The electron from the ground sate of Mn^{2+} is first excited into the higher energy levels of Mn^{2+}. The excited free electron then relaxes to the $^4T_1(^4G)$ excited state through $^4E(^4D)$, $^4T_2(^4D)$, $^4A_1(^4G)$,$^4E(^4G)$, and $^4T_2(^4G)$ intermediate energy levels of Mn^{2+} by a nonradiative process, followed by a radiative transition from the $^4T_1(^4G)$ to the $^6A_1$ ground state giving rise the red emission centered at 636 nm of Mn^{2+} in the $KMgBO_3$ host lattice. In addition, the efficient energy transfer from the host lattice to the Mn^{2+} ion also results in the emission of Mn^{2+} centered at 636 nm. Based on the above two ways, a strong emission band is observed in $KMgBO_3$:Mn^{2+}.

3.3 Concentration effect of $KMgBO_3$:Mn^{2+}

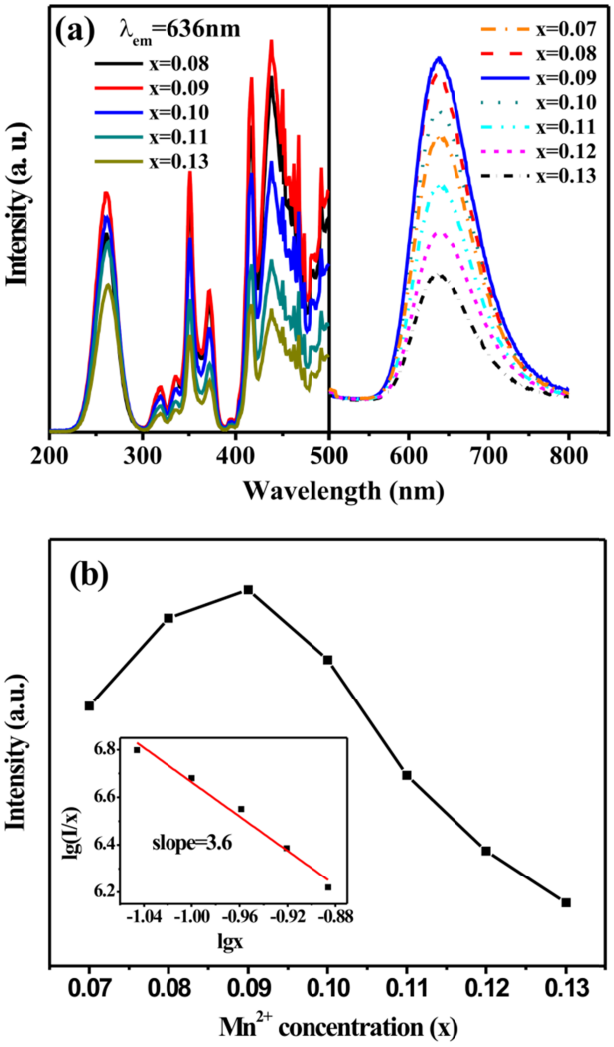

Fig. 4. (a) Excitation and emission spectra of KMgBO3:Mn2+ phosphors with different Mn2+ doping concentrations. (b) Emission intensity vs. Mn2+ concentration (x) of KMgBO3:xMn2+ phosphor. The inset shows the dependence of lg(I/x) on lgx.

Fig. 4(a) shows the excitation spectra and the emission spectra of $KMgBO_3$:Mn^{2+} phosphors with different Mn^{2+} doping concentration, respectively. The shape and the position of the Mn^{2+} excitation peaks are almost independent of the Mn^{2+} doping concentration. However, the concentration of Mn^{2+} affects its excitation intensity intensely because this is determined by energy transfer efficiency between the host lattice and Mn^{2+}. The maximum CTS excitation intensity is obtained for the sample doped with 9% Mn^{2+}. In addition, it can be observed that the ratio between the intensities of Mn^{2+} excitation bands and CTS excitation band increase with the

Mn^{2+} concentration increase before the maximum doped concentration of Mn^{2+} (9 mol%).

As for the PL spectra of $KMgBO_3:Mn^{2+}$ phosphors with different Mn^{2+} doping concentration, the positions of the emission bands are independent of the Mn^{2+} contents, and the emission intensities of the Mn^{2+} ions first increase with increasing the doping concentration, reaching a maximum at the concentration of 9 mol% Mn^{2+}, and then decrease with the doping concentration increase because of the concentration quenching effect. The critical distance (R_c) can be estimated by the following equation:[31]

$$R_c = 2\left(\frac{3V}{4\pi x N_c}\right)^{1/3} \quad (2)$$

where x refers to the quenching concentration, V denotes the volume of the unit cell, N_c is the number of Mg^{2+} in the unit cell. In this study, x is 0.09, N_c is 4, V is 321.33 $Å^3$. Thus, the critical distance of Mn^{2+} doped $KMgBO_3$ is about 11.95 Å.

According to Dexter's theory, multipolar interactions intensity can be expressed by the PL intensity. The emission intensity (I) per activator of $KMgBO_3:Mn^{2+}$ phosphor can be deduced by [32]

$$I/x = k/\left[1+\beta(x)^{\theta/3}\right] \quad (3)$$

where I is the emission intensity, x is the concentration of activator, k and β are the constants for a given excitation wavelength and crystal structure. The values of θ are 6, 8, 10, corresponding to dipole-dipole, dipole-quadrupole, and quadrupole-quadrupole interaction, respectively. When x exceeds critical concentration, the equation can be simplified to $\frac{I}{x} = K'\left[\beta(x)^{\theta/3}\right]^{-1}$. So θ can be determined from the ratio of lg(I/x) to lgx. As shown in the inset of Fig. 4(b), the value of θ can be calculated to be 10.2 from the slop of -3.4, which is close to 10, indicating that the concentration quenching is mainly dominated by the quadrupole-quadrupole interaction in Mn^{2+} doped $KMgBO_3$ phosphors.

3.4 Thermal quenching properties of $KMgBO_3:Mn^{2+}$

Temperature-dependent PL spectra are measured to investigate the thermal quenching properties of the $KMgBO_3:Mn^{2+}$. Fig. 5(a) shows the temperature-dependent PL spectra of $KMgBO_3:0.09Mn^{2+}$ excited at 438 nm. Fig. 5(b) displays and compares the thermal quenching properties of $KMgBO_3:0.09Mn^{2+}$ phosphor and the commercial red $SrS:Eu^{2+}$phosphor. The thermal stability of $KMgBO_3:Mn^{2+}$ is nearly the same as that of SrS: Eu^{2+} in the temperature range from RT to 125 °C, which is within the LED operating temperature. The fast decrease of the emission at the different temperature is possible because of the hygroscopic nature of borates. However, the hygroscopicity for $KMgBO_3:Mn^{2+}$ is not a severe problem for its potential LED application because LED phosphors are sealed in the transparent silicone resin in LED cell during measurements.

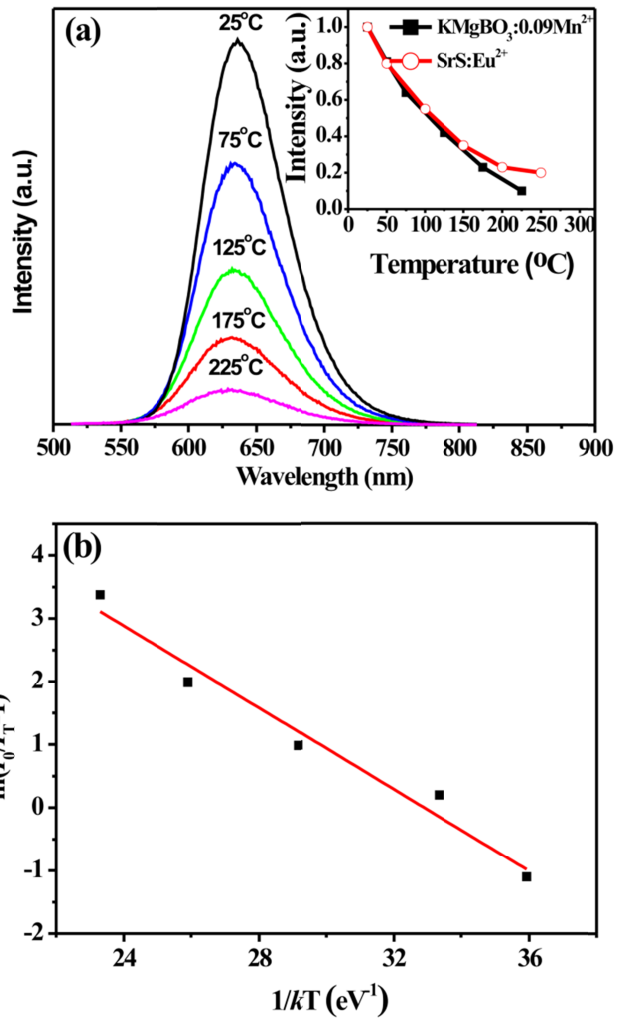

Fig. 5. (a) Temperature-dependent PL spectra of KMgBO3:0.09Mn2+ phosphor (λex=438nm). (b) Normalized PL intensity as a function of temperature. As a comparison, thermal quenching data of SrS:Eu2+excited at 460 nm are also measured as a reference. Inset is the ln (I0/IT-1) vs. 1/kBT activation energy graph for thermal quenching of KMgBO3:0.09Mn2+.

Generally, the luminescence thermal quenching effect is attributed to the non-radiative relaxation through the crossing point between the excited state and the ground state in the configurational coordinate diagram. The non-radiative transition probability is strongly dependent on temperature, resulting in the decrease of emission intensity. The decrease of the emission intensity of the phosphors depended on the temperature and can expressed by

$$ln\left(\frac{I}{I_0}\right) = ln\,A - \frac{E_a}{kT} \quad (4)$$

where I_0 and I are the luminescence intensity of $KMgBO_3:0.09Mn^{2+}$ at room temperature and the testing temperature, respectively. A is a constant; k is the Boltzmann

constant (8.617×10^{-5} eV K^{-1}). Ea was obtained to be 0.32 eV (inset in Fig. 5 (b)).

3.5 Decay properties of $KMgBO_3:Mn^{2+}$

In order to check the potential application of synthesized $KMgBO_3:Mn^{2+}$ in lighting, the luminescence decay curves of $KMgBO_3:xMn^{2+}$ (x=0.08, 0.09, 0.10, 0.11, 0.12, 0.13) are measured under the excitation of 438 nm and are represented in Fig. 6. The decay curves can be well fitted with first-order exponential decay mode by the following equation: [5]

$$I = I_0 \exp(-t/\tau) \quad (5)$$

where I_0 and I are the luminescence intensities at time 0 and t, τ is the fluorescence lifetime. Obviously, there is only one type of Mn^{2+} emission site in the host from the fitting results, which is in good agreement with the structural and PL studies. The luminescence decay lifetime is determined to be 4.09 ms, 3.71 ms, 3.65 ms, 2.96 ms, 2.64 ms, and 2.43 ms for $KMgBO_3:xMn^{2+}$ with x=0.08, 0.09, 0.10, 0.11, 0.12, and 0.13. The results are consistent with the fact that the decay time of the Mn^{2+} ions is several to tens of milliseconds [10]. It can be found that the decay lifetime decrease with the Mn^{2+} dopant contents increase, which is because of the superexchange interactions between Mn^{2+} close ion pairs.[11,33]

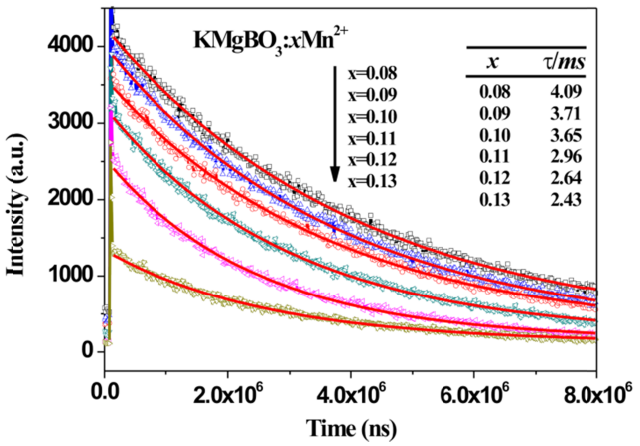

Fig. 6. Room temperature decay curves of $KMgBO_3:xMn^{2+}$ with Mn^{2+} contents (x=0.08, 0.09, 0.10, 0.11, 0.12, 0.13) (excited at 438nm, monitored at 636nm).

3.5 Quantum efficiency and CIE coordinates

Quantum efficiency is requested for LED phosphor, which is related to the overall electrical-to-optical conversion efficiency of the entire LED-phosphor package. To determine the absolute quantum efficiency of photo-conversion for the $KMgBO_3:Mn^{2+}$ phosphor, the integrated sphere method is applied for the measurements of optical absorbance (A) and quantum efficiency (η_{int}) of the phosphors. The absorbance can be calculated by using the following equation:

$$A = \frac{L_0(\lambda) - L_i(\lambda)}{L_0(\lambda)} \quad (6)$$

where $L_0(\lambda)$ is the integrated excitation profile when the sample is diffusely illuminated by the integrated sphere's surface, $L_i(\lambda)$ is the integrated excitation profile when the sample is directly excited by the incident beam. Furthermore, the internal quantum efficiency (η_{int}) of the phosphors can be calculated by

$$\eta_{int} = \frac{E_i(\lambda) - (1-A)E_0(\lambda)}{L_e(\lambda)A} \quad (7)$$

where $E_i(\lambda)$ is the integrated luminescence of the powder up direct excitation, and $E_0(\lambda)$ is the integrated luminescence of the powder excited by indirect illumination from the sphere. The term $L_e(\lambda)$ is the integrated excitation profile obtained from the empty integrated sphere (without the sample present). The internal quantum efficiency (η_{int}) of $KMgBO_3:0.09Mn^{2+}$ is found to be 52.2%.

The Commission International de l'Eclairage (CIE) chromaticity coordinates for $KMgBO_3:Mn^{2+}$ excited at 438nm are shown in Fig. 8. The CIE chromaticity coordinates of $KMgBO_3:Mn^{2+}$ are (0.66, 0.34), which is very close to the standard red color (0.66, 0.33). It indicates that the red color emitted by $KMgBO_3:Mn^{2+}$ is with high purity and high color saturation. Together considering the absorption spectra, PLE/PL spectra, temperature-dependent PL spectra, decay time, and CIE coordinate and color saturation, the Mn^{2+} single doped Mg-based phosphor $KMgBO_3:Mn^{2+}$ is a potential red phosphor for UV LED lighting and the emission intensity will increase with the LED power increase.

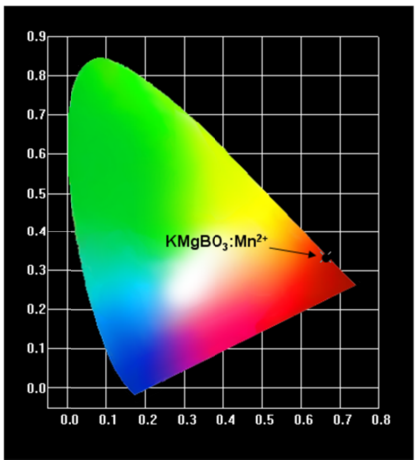

Fig. 7. CIE chromaticity diagram for $KMgBO_3:0.09Mn^{2+}$ excited at 438 nm.

4. Conclusion

A series of novel red phosphor rare earth free red emitting $KMgBO_3:Mn^{2+}$ are synthesized by the solid-state reaction, and the site occupancy of Mn^{2+} in $KMgBO_3$ host and the photoluminescence performance are investigated. The Rietveld refinement result shows that Mn^{2+} ions are preferred to occupy the Mg^{2+} site (4a). The strong absorption of the $KMgBO_3:Mn^{2+}$ is ascribed to the strong relaxation of spin and parity forbidden of Mn^{2+}, and the red emission of Mn^{2+} centered at 636 nm is from the transition of $^4T_1(^4G) \rightarrow {}^6A_1(^6S)$. The shape and peak

positions of emission bands are independent of the excitation wavelength. Efficiently excitation of Mn^{2+} d-d transition can be easily observed in the range of 300-475 nm. The red-shift of Mn^{2+} emission is because of the strong crystal field environment. Temperature-dependent PL properties indicate that the thermal quenching properties of $KMgBO_3:Mn^{2+}$ is nearly the same as the commercial red phosphor $SrS:Eu^{2+}$ in the range from RT to 125 ^oC. The concentration quenching occurs when the Mn^{2+} doping concentration is above 9 mol % and the critical distance is 11.95 Å. The potential applications of the $KMgBO_3:Mn^{2+}$ phosphors have been pointed out based on the absorption spectra, excitation and emission spectra, thermal quenching properties, decay properties, and CIE coordination and color saturation.

Acknowledgements

This work was supported by National Natural Science Foundation of China (61274053, 90922037 and 51372121), Natural Science Foundation of Tianjin (14JCYBJC17800), and the Program for New Century Excellent Talents in University of China (NCET-11-0258). We thank Mrs. Y. P. Xu of A02 group, Institute of Physics, Chinese Academy of Science for step XRD measurement.

Notes and references

[a] The MOE key laboratory of weak-Light Nonlinear Photonics, School of Physics, Nankai University, Tianjin 300071, China.

[b] Institute of Photo-electronic Thin Film Devices and Technology, Key Laboratory of Photo-electronic Thin Film Devices and Technology of Tianjin, Nankai University, Tianjin 300071, PR China. Email: yizhang@nankai.edu.cn, Tel: +86-22-23508572-8018, Fax: +86-22-23508912

[c] Tianjin Key Laboratory of Photoelectronic Materials and Device, Tianjin University of Technology, Tianjin 300191.

†Electronic Supplementary Information (ESI) available: Rietveld refinement results on $KMgBO_3:0.09Mn^{2+}$. See DOI: 10.1039/b000000x/

1. K. Sharma, K. H. Son, B. Y. Han, K. S. Sohn, Adv. Funct. Mater., 2010, **20**, 1750.
2. A. Setlur, J. J. Shiang, U. Happek, *Appl. Phys. Lett.*, 2008, **92**, 081104.
3. P. F. Smet, A. B. Parmentier, D. Poelman, *J. Eelectrochen. Soc.*, 2011, **158**, R37.
4. Y. R. Shi, Y. Wen, M. Que, G. Zhu, Y. H. Wang, *Dalton Trans.*, 2014, **43**, 2418
5. G. Blasse, B. C. Grabmaier, *Luminescent Materials* (Spring-Verlag: Berlin, 1994).
6. C. Huang, P. Wu, J. Lee, T. Chen, *J. Mater. Chem.*, 2011, **21**, 10489.
7. J. Nara, S. Adachi, *J. Appl. Phys.*, 2013, **113**, 033519.
8. T. S. Chan, R. S. Liu, I. Baginskiy, *Chem. Mater.*, 2008, **20**, 1215.
9. J. Duan, A. C. Delsing, H. T. Hintzen, *Chem. Mater.*, 2009, **21**, 1010.
10. M. Shang, G. Li, D. Yang, X. Kang, C. Peng, J. Lin, *Dalton Trans.*, 2012, **41**, 8861.
11. J. Lv, F. Du, R. Zhu, Y. Lin, H. J. Seo, *J. Mater. Chem.*, 2011, **21** 16398.
12. R. Pazik, K. Zawisza, A. Watras, K. Maleszka-Baginska, P. Boutinaud, R. Mahiou, P. J. Deren, *J. Mater. Chem.*, 2012, **22**, 22651.
13. S. Yuan, Y. Yang, X. Zhang, F. Tessier, F. Chevire, J. Adam, B. Moine, G. Chen, *Opt. Lett.*, 2008, **33**, 2865.
14. L. Wu, X. L. Chen, H. Li, M. He, Y. P. Xu, X. Z. Li, *Inorg. Chem.*, 2005, **44**, 6409.
15. Y. Zhang, W. Liu, M. Ji, B. Wang, Y. Kong, J. Xu, *Opt. Mater. Express*, 2012, **2**, 92.
16. L. Wu, Y. Zhang, M. Y. Gui, P. Z. Lu, L. X. Zhao, S. Tian, Y. F. Kong, J. J. Xu, *J. Mater. Chem.*, 2012, **22**, 6463.
17. W. R. Liu, C. H. Huang, C. P. Wu, Y. C. Chiu, Y. T.Yeh, T. M. Chen, *J. Mater. Chem.*, 2011, **21**, 6869.
18. L. Wu, J.C. Sun, Y. Zhang, S.F. Jin, Y.F. Kong, J.J. Xu, *Inorg. Chem.*, 2010, **49**, 2715.
19. R. D. Shannon, *Acta Crystal. A*, 1976, **32**, 751.
20. H. M. Rietveld, *Acta Crystallogr.*, 1967, **22**, 151.
21. H. M. Rietveld, *J. Appl. Cryst.*, 1969, **2**, 65.
22. J. Rodriguez-Carvajal, FULLPROF2000, (LLB, France, 2001).
23. Y. Nobuhiko, *J. Phys. Soc. Jpn.*, 1973, **35**, 1089.
24. Q. H. Zhang, J. Wang, C. W. Yeh, W. C. Ke, R. S. Liu, J. K. Tang, M. B. Xie, H. B. Liang, Q. Su, *Acta Mater.*, 2010, **58**, 6728.
25. L. E. Orgel, *J. Chem. Phys.*, 1955, **23**, 1004
26. J. Wang, S. B. Wang, Q. Su, *J. Mater. Chem.*, 2004, **14**, 2569.
27. T. W. Kuo, W. R. Liu, T. M. Chen, *Opt. Express*, 2010, **18**, 8187.
28. M. Shinn and W. Sibley, *Phys. Rev. B*, 1984, **29**, 3834
29. J. S. Kim, P. Jeon, J. Choi, H. Park, S. Mho, and G. Kim, *Appl. Phys. Lett.*, 2004, **84**, 2931.
30. W. J. Yang, L. Luo, T. M. Chen, N. S. Wang, *Chem. Mater.*, 2005, **17**, 3883.
31. G. Blasse, *Philips Res. Rep.*, 1969, **24**, 131.
32. L. G. Van Uitert, *J. Electrochem. Soc.*, 1967, **114**, 1048.
33. E. C. Machado, L. Prado, L. Gomes, J. M. Prison, J. R. Martinelli, *J. Non-Cryst. Solids*, 2004, **348**, 113.